Cement & Concrete Composites 33 (2011) 225–232

Contents lists available at ScienceDirect

Cement & Concrete Composites

journal homepage: www.elsevier.com/locate/cemconcomp

Effects of natural weathering on microstructure and mineral composition of cementitious roofing tiles reinforced with fique fibre

G.H.D. Tonoli [a,*], S.F. Santos [b], H. Savastano Jr. [b], S. Delvasto [c], R. Mejía de Gutiérrez [c], M. del M. Lopez de Murphy [d]

[a] Structural Engineering Department, Escola de Engenharia de São Carlos, Universidade de São Paulo, Brazil
[b] Food Engineering Department, Faculdade de Zootecnia e Engenharia de Alimentos, Universidade de São Paulo, Brazil
[c] Composite Materials Group, Escuela de Ingeniería de Materiales, Universidad del Valle, Colombia
[d] Civil and Environmental Engineering Department, The Pennsylvania State University, USA

ARTICLE INFO

Article history:
Received 22 January 2010
Received in revised form 13 August 2010
Accepted 15 October 2010
Available online 26 October 2010

Keywords:
Air permeability
Fibre-cement
Durability
Cementitious corrugated sheets
Vegetable fibres
Forchheimer's equation

ABSTRACT

The objective of the present work was to evaluate the effects of 14 years of weathering exposition on the microstructure and mineral composition of cementitious roofing tiles, still in service, reinforced with fique fibres (*Furcrae gender*). The results show that tiles under weathering exposition presented higher water absorption and apparent void volume than tiles under laboratory exposition. The continuous hydration of cement and natural carbonation filled the smaller pores but contrarily the large pores remained in the porous fibre to matrix interface in the samples exposed to weathering. On the other hand, their microstructure presented lower air permeability than samples aged in the internal environment of the laboratory. Besides, in the weathering aged tiles takes place a more intensive hydration process as it was identified greater amount of hydrated phases than in the laboratory aged specimens. The present results contribute to understanding the consequences of tropical weathering on the fibre-cement degradation.

1. Introduction

Since ancient times, approximately 3500 years ago, brittle building materials, e.g. clay sun baked bricks, were reinforced with vegetable fibres. However, the concept of vegetable fibre reinforcement in cement-based materials was developed in 1970s, when vegetable fibres were evaluated as substitutes of manufactured fibres and asbestos fibres [1,2]. Natural vegetable fibres (cellulose pulp, sisal, bamboo, fique, hemp, flax, jute and ramie, for example) are used in regions where these materials are readily available. Motivations for their use include decreased costs and meeting the needs of sustainability and ecology.

Composites with vegetable fibres are important for construction of inexpensive buildings in developing regions of the world. On the contrary, the use of synthetic fibres frequently involves higher costs and greater consumption of energy in the processing of fibre reinforced cementitious composites [3]. According to Swamy [4], the use of composites reinforced with vegetable fibres in flat sheets, roofing tiles and pre-manufactured components can represent significant contribution to the infrastructure in developing countries. It has been demonstrated that fique fibre, which is a commercially available natural fibre in Colombia, is appropriate for low cost housing applications when incorporated into a matrix based on Portland cement, being suitable for making elements of various shapes using simple production processes [5–7]. Another concern is the durability of alternative products, as well as their compatibility to the service life of building components in general [8].

The present study was carried out to evaluate the changes occurring in the microstructure and in the chemical composition of tiles reinforced with lignocellulosic fibres when exposed to 14 years of natural weathering conditions. For comparison, a set of tiles was made and kept under laboratory conditions during the same period prior to testing.

2. Experimental

2.1. Characteristics of the fique fibres

Fique fibre or cabuya (*Furcrae gender*) is a Colombian native vegetable fibre with similar characteristics to sisal. It has been demonstrated that the fique fibre is suitable for cementitious materials in low cost housing applications [5–7] and for fibre reinforcement of concrete [9].

* Corresponding author. Fax: +55 19 3565 4114.
E-mail addresses: gustavotonoli@yahoo.com.br (G.H.D. Tonoli), sfsantos1@usp.br (S.F. Santos), holmersj@usp.br (H. Savastano Jr.), silviodelvasto@hotmail.com (S. Delvasto), rudeguti@hotmail.com (R. Mejía de Gutiérrez), mmlopez@engr.psu.edu (M. del M. L. de Murphy).

0958-9465/$ - see front matter © 2010 Elsevier Ltd. All rights reserved.
doi:10.1016/j.cemconcomp.2010.10.013

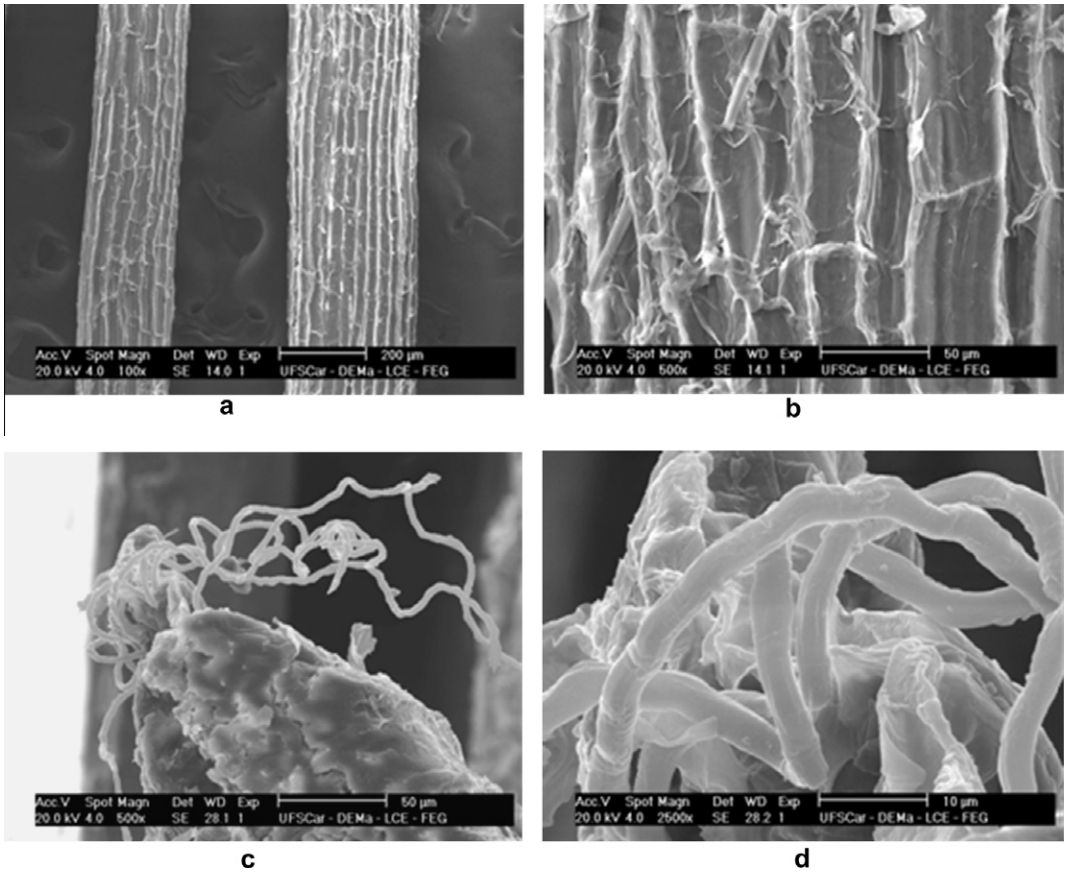

Fig. 1. Scanning electron micrographs of the fique fibres. Fibre cells linked to each other by the middle lamellae (a and b). Approximately 4 μm thick loose filaments or microfibrillae (c and d).

Fig. 1 shows scanning electron micrographs (SEM) of the fique fibres. The fibres are thicker than 0.2 mm (Fig. 1a). In the outer wall the fibrillae have a reticulated structure (Fig. 1b). The fibre consists of a number of walls built up of fibrillae. The fibrillae are, in turn, built up of microfibrillae (Fig 1c and d).

A fique fibre in cross-section is built up of many fibre cells (3–4 μm of diameter each). The fibre cells are linked together by the lamellae, which consist of hemicellulose, lignin and pectin. Some fibre properties are listed in Table 1.

2.2. Production of the roofing tiles

Fibre-cement corrugated roofing sheets with nominal dimensions of 1830 mm long, 920 mm wide, 6 mm thick, and 57 mm crest height were produced by a hand casting process. The matrix of the roofing tiles used in this study consisted of ordinary Portland cement, hydrated lime and river sand in the following proportion 1:0.125:0.33 by mass. The water–cement ratio was 0.35. The properties of the Portland cement can be seen in Table 2. Hydrated lime with a CaO content of 72.6% and LOI of 25.4% was incorporated into the mix in form of putty lime with 50% of solids. A river siliceous sand with a maximum grain diameter of 0.5 mm and fineness modulus of 2.93 was used. It was used 4% (3% of the total mass of solids) of short discontinuous fique fibres that were previously treated by immersion into a boiling lime solution for 5 min. The fibres were cut to a desired average length of 15 mm.

The cement, sand and fibres were mixed by hand using a shovel, then the water with the putty lime were added to the mix to get a plastic consistency. Afterwards, the fibre reinforced mortar was poured in a mould to shape a plane sheet of 8 mm thick. Extra mortar was tamped and levelled off. The frame of the mould was made

Table 1
Characteristics of the fique fibres [7].

Properties	Range	Average
Thickness (mm)	0.16–0.42	0.24
Apparent density (g/cm^3)	–	0.723
Real density (g/cm^3)	–	1.47
Water absorption (%)	–	60
Equilibrium relative humidity (%), absorbency	–	8.12
Lignin (%)	–	10.1
Cellulose (%)	–	70.0
Modulus of elasticity (GPa)	8.2–9.1	
Ultimate elongation (%)	–	9.8
Tensile strength (MPa)	43–571	132.4

Table 2
Chemical composition and physical and mechanical properties of ordinary Portland cement.

Chemical composition (% by mass)		Physical and mechanical properties	
SiO_2	21.07	Specific gravity (g/cm^3)	3.12
Al_2O_3	5.41	Blaine fineness (m^2/kg)	368
Fe_2O_3	4.69	Fineness: 74 μm (%-retained)	4.0
CaO	63.04	Setting time (initial set/min)	95
MgO	2.02	Compressive strength of mortar cubes – (ASTM C109)	
Na_2O	0.16	After 1 day (MPa)	10.1
K_2O	0.18	After 3 days (MPa)	23.3
SO_3	1.51	After 7 days (MPa)	36.0
LOI	1.52	After 28 days (MPa)	46.7

out of an aluminium profile, the sides of the mould could easily be opened and secured. The mould was located on a flat surface covered with a plastic foil. Then, the mould with the fresh plane sheet was placed on a vibration table and compacted during 1 min. After compaction, the plane sheet was transferred to a plastic corrugated sheet to get a wavy form. The plasticity of the fibre reinforced mortar allowed that the sheet take this corrugated form. Then, the fresh corrugated tile was left to harden in a shaded humid environment for twelve hours. After this, the roofing corrugated sheet was cured in water during 20 days.

2.3. Weathering conditions

Tiles were exposed during 14 years under natural weathering conditions at a small prototype house roof structure (Fig. 2), in Cali, Colombia (latitude 03°24′N, longitude 76°38′W, and mean elevation of around 970 m). During the period under consideration the maximum and minimum temperatures were 32 °C and 17 °C, respectively, average wind speed was between 1.2 km/h and 2.0 km/h, respectively, rainfall was approximately 1300 mm/year, maximum and minimum relative humidity were 84.2% and 62.5%, respectively, and solar radiation was around 376 cal/cm^2/day. Part of the tiles was kept during the same period (14 years) under protected environment in laboratory (∼24 °C and ∼65% relative humidity) and used as reference material.

2.4. Microstructure characterization tests

Tiles of each exposure condition were evaluated on permeability properties (porosity and air permeability) and chemical composition. Water absorption (WA), apparent void volume (AVV) and bulk density (BD) results were obtained under vacuum during 2 h (∼80 kPa gauge) after 24 h immersed in tap water. Real density was measured using a Quantachrome multipicnometer, model MVP-6DC.

Scanning electron microscopy (SEM) was applied for the characterization of fibre–matrix interface and the transition zone. A backscattered electron (BSE) detector was applied to observe the morphological features of cut and polished surfaces. The BSE imaging permits the easy identification of cementitious phases since electron scattering goes with the atomic number. Dark and light areas are related to lighter and heavier elements, respectively. Energy Dispersive Spectrometry (EDS) analyses were performed in order to identify the chemical composition in different spots on the same polished surface specimens. The preparation of specimens for BSE and EDS was accomplished with vacuum (25 kPa gauge) impregnation using epoxy resin (MC-DUR1264FF type). BSE EDS samples were grinded with silicon carbide (SiC) grinding paper with sequential grit sizes of 120, 320 and 500 for 4 min each, using ethanol (Struers DP lubricant) as lubricant. A final polishing was carried out using in turn 8–4 μm, 4–2 μm and 1–0 μm diamond polishing compound during 6 min each size. Polished samples were carbon coated before being analysed in a LEO Leika S440 scanning electron microscope with an acceleration voltage of 20 kV and current of 150 mA, as described elsewhere [10].

Mercury intrusion porosimetry (MIP) was performed using Micrometrics 9320 Poresizer with operation pressures of up to 200 MPa. The assumptions were 0.495 g/cm^2 mercury surface tension and 13534 kg/m^3 mercury density. Equilibration time in both low and high pressures was 10 s. The advancing/receding contact angle was assumed to be 130°. The amount of mercury introduced at each pressure interval was recorded. Specimens were cut with a cubic side length of approximately 5 mm, dried at 70 °C for 24 h and stored in an air-tight recipient prior to evaluation. Sample mass was approximately 2 g. The technique was adopted in order to evaluate the pore size distribution as usually applied in the characterization of cement-based materials [11,12].

Experimental evaluation of air permeability at room temperature (25–30 °C) was conducted in a permeameter, as described by Innocentini et al. [13]. The sample was fixed between two chambers with a testing area of 4.91×10^{-4} m^2. The experiments evaluated the easiness of airflow passing through the sample thickness (around 8 mm) by measuring the exit air velocity in response to the variations of the inlet pressure applied. Permeability tests were performed on at least three specimens for each treatment. Samples were previously dried in a ventilated oven at 100 °C. The moisture was removed primarily to prevent any influence of water on the measurements. The permeability constants k_1 and k_2 were obtained by fitting the experimental data using Forchheimer's equation (Eq. (1)), expressed for flow of compressible fluids [14]:

$$\frac{P_i^2 - P_o^2}{2P_oL} = \left(\frac{\mu}{k_1}\right)v_s + \left(\frac{\rho}{k_2}\right)v_s^2 \tag{1}$$

where P_i and P_o are the absolute inlet and outlet air pressures respectively; v_s is the fluid velocity; L the sample thickness; μ the fluid viscosity (air viscosity $\sim 1.8 \times 10^{-5}$ Pa s); and ρ the fluid density (air density $\sim$1.08 kg/m^3). The parameters k_1 and k_2 are the Darcian and non-Darcian permeability constants respectively.

The permeability constant k_1, or Darcian constant, represents the viscous effect of the shearing (friction and interactions between fluid and porous media); the permeability constant k_2, or non-Darcian constant, reflects the tortuosity of the porous media when the shearing velocity is high [15]. The higher the k_1 and k_2 values, the higher the permeability of the porous media.

Fig. 2. Small prototype house roof structure.

2.5. Chemical phase characterization of the roofing tiles

The chemical phases present in the roofing tiles samples were analysed by X-ray diffraction (XRD) in Rigaku Rotoflex RU-200B equipment with horizontal goniometer, multipurpose camera and monochromator. The conditions of operation were voltage of 50 kV, electric current equal to 100 mA, velocity of 1°/min and step of 0.02°. Samples used in this analysis were ground and passed through the 45 μm screen.

Thermogravimetric analyses (TG) were conducted with a Netzsch STA409 PG using a sample mass of approximately 1.0 g and nitrogen atmosphere (flow ratio = 60 mL/min), heating ratio of 10 °C/min up to the maximum temperature of 1000 °C. Prior to testing, the samples were dried at 40 °C under negative pressure (60 kPa) during 24 h to remove any moisture.

3. Results and discussion

3.1. Changes in the microstructure of the tiles

Despite of being exposed to the weather, there is no visible sign of decay in the corrugated sheets, which have been mounted on a small prototype house roof structure. Until now, the roof stability and shape are maintained. It was observed a tendency of high real density of the matrix of tiles under natural weathering exposition (Table 3). This could be the consequence of the formation of additional crystalline cementitious phases in these tiles.

Table 4 presents the physical properties of the specimens from laboratory and natural weathering exposition. The increase of the water absorption and apparent void volume for the roofing tiles aged under natural weathering exposition could be the consequence of the leaching of some less stable cementitious products, which decreased the bulk density of the specimens. Similarly, the mercury intrusion data (Table 5) shows the lower bulk density and apparent (skeletal) density of the specimens from weathering exposition. It can be seen the lower total pore area of the weathering exposed tile and that the average pore diameter increased around 50% in relation to the tile aged in laboratory.

In Fig. 3 it is presented the consequence of weathering exposition of the tiles on the fibre–matrix interface (transition zone). The fibres are placed longitudinally and they are detached from the matrix (arrows) due to the shrinking upon drying. The fibre to matrix interface in weathering exposed tile (Fig. 3b) was much damaged in relation to the fibre to matrix interface in the tiles aged in laboratory (Fig. 3a). As reported by Savastano Jr. et al. [10], this damage in the interface is provoked by stresses during the fibre volume changes under continuous alternation of wetting, drying and carbonation in the tiles exposed to natural weathering. Matrix microcracking close to the fibres generates greater spaces or pores on the transition zone of tiles exposed to weathering, which also explains the higher porosity found in these tiles in relation to laboratory aged tiles (Tables 4 and 5).

Table 3
Real density of the ground tiles.

Property	Laboratory	Natural weathering
Real density (g/cm^3)	2.65 ± 0.01	2.70 ± 0.12

Table 4
Average values and standard deviations for water absorption (WA), apparent void volume (AVV) and bulk density (BD) of the samples of the roofing tiles.

Physical property	Laboratory	Natural weathering
Water absorption (%)	11.6 ± 1.3	13.5 ± 0.2
Apparent void volume (%)	22.9 ± 2.1	25.6 ± 0.2
Bulk density (g/cm^3)	1.97 ± 0.04	1.89 ± 0.02

Table 5
Mercury intrusion porosimetry data for the tiles.

Mercury intrusion porosimetry data	Laboratory	Natural weathering
Total intrusion volume (mL/g)	0.030 ± 0.004	0.032 ± 0.006
Total pore area (m^2/g)	4.7 ± 0.5	3.4 ± 1.2
Median pore diameter – volume (μm)	0.036 ± 0.001	0.115 ± 0.013
Median pore diameter – area (μm)	0.013 ± 0.001	0.013 ± 0.001
Average pore diameter – 4 V/A (μm)	0.025 ± 0.001	0.038 ± 0.006
Bulk density (g/cm^3)	1.99 ± 0.01	1.93 ± 0.02
Apparent (skeletal) density (g/cm^3)	2.11 ± 0.02	2.06 ± 0.01
Porosity (%)	5.87 ± 0.64	6.07 ± 1.17

Fig. 4 presents the pore size distribution curve of the specimens from laboratory and natural weathering exposition. The peak between 10 nm and 100 nm is related to the cement paste (matrix) and the peaks between 100 nm and 1000 nm are capillary pores resulting from the manufacturing process. The amount of voids inside the fibre strands and cellulose fibres in fibre-cement actively influences the peak between 100 nm and 1000 nm [16], but can also be related to the pores in the fibre to matrix interface (transition zone) (Fig. 3b). Weathering exposed tile revealed a coarsening of pores greater than 100 nm in comparison with the tile aged in laboratory (Fig. 4). Coarsening has been associated to the SiO_2 (gel) formation during carbonation of C–S–H [17] and leaching of the cement matrix [18] or unstable phases of carbonates [19].

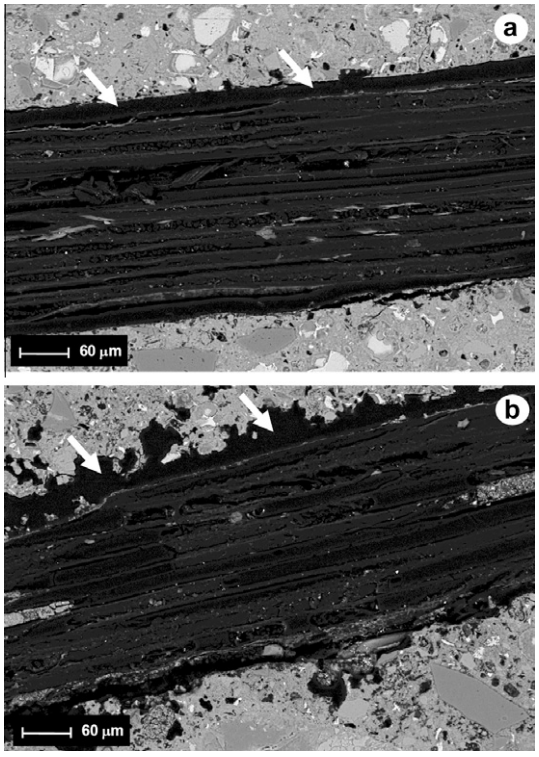

Fig. 3. Back scattering electrons (BSE) image of the fibre to matrix interface (arrows) in 14 years old tile: (a) aged in laboratory, and (b) under natural weathering exposition.

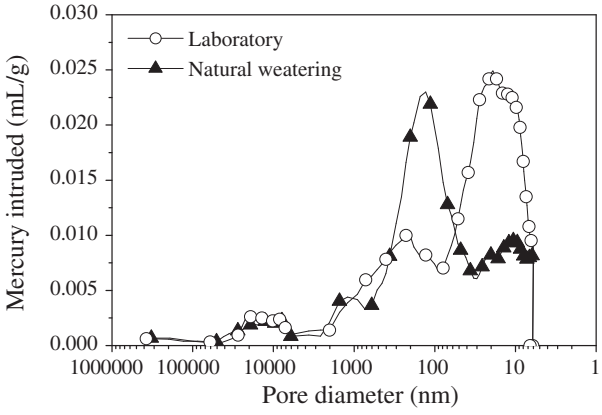

Fig. 4. Pore size distribution for specimens aged in laboratory and under natural weathering exposition.

During the weathering exposition the continuous hydration of the cement led to the reduction of matrix voids (densification showed in Table 3). Natural carbonation filled the small pores (below 100 nm) in the matrix, but remained the large pores, which increased the average pore diameter, as described by Mehta and Monteiro [12].

The air permeability is a physical property of extreme importance to the development of durable elements to civil construction. The permeability can be associated with the resistance to the penetration of degradation agents and also with the microstructure properties (e.g. particle packing and permeable pores). In Fig. 5 it can be observed that higher pressure is necessary to the same air velocity in the tiles aged under natural weathering exposition. Furthermore, the k_1 and k_2 values decreased in the case of tiles under natural weathering exposition in relation to laboratory exposition (Table 6). The decrease of k_1 indicates that friction and interactions between fluid and porous media increased [19]. The non-Darcian constant, k_2, decreased in the case of natural weathering exposition, which can be interpreted as the increase of the tortuosity of the porous structure [19].

The primary cause of vegetable macrofibre degradation in a cement based matrix is assumed to be the chemical decomposition of lignin and hemicelluloses in the middle lamella [20], which have the function of bonding in the individual fibres [21]. The alkaline pore water in fibre-cement dissolves lignin and the hemicelluloses in the middle lamella of the fique macrofibres, which turns them susceptible to loses in reinforcing capacity in fibre-cement composites. It is generally held that decomposition of the cellulose fibre in an alkaline environment can take place in accordance with two different mechanisms. One is the peeling-off mechanism which occurs at the end of the molecular chain. The other is alkaline hydrolysis. This induces the molecular chains to divide, and the degree of polymerization decreases [20]. Another cause of vegetable fibre degradation is that fibre cells can be filled with cement hydration products, which lead the fibre to losing its flexibility.

Fig. 6 presents SEM-BSE micrographs of the fibre cross-section in tiles aged in protected environment (laboratory). It can be seen in Fig. 6a the energy dispersive X-ray spectroscopy (EDS) analysis indicating that the fique fibre was almost free from cement hydration products (for example, phases rich in calcium).

In the tiles aged under natural weathering (Fig. 7), it is evidenced the calcium re-precipitation both in the fibre surroundings (fibre–matrix interface) and into the fibre cavities (lumen). Fig. 7a depicts the EDS spectra into the fibre cavities showing the higher presence of calcium in comparison to Fig. 6a. In the tiles exposed to the natural weathering the rain water absorbed by the tiles led to the dissolution of some soluble cement hydration products in the bulk of the tiles. Part of these cement products was then carried out by the water and deposited into the fibre cavities, leading to the accelerated mineralization and loss of fibre flexibility. Additionally, after 14 years of weathering exposition some changes in the fibre chemical composition can be expected, as the reduction in the amount of lignin and hemicellulose [22], which also decreases the fibre strength.

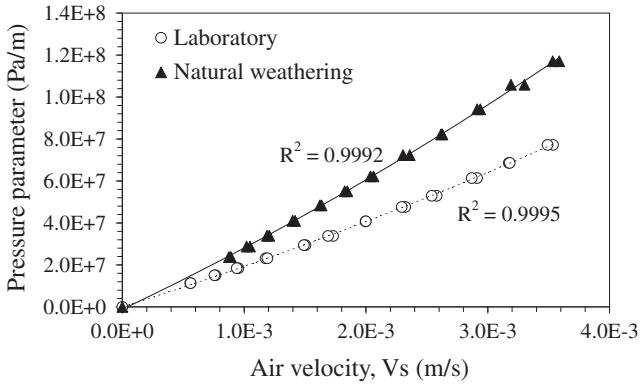

Fig. 5. Forchheimer's equation fitted to experimental data of specimens aged in laboratory condition and under natural weathering exposition according to the expression for compressible fluids.

Table 6
Darcian (k_1) and non-Darcian (k_2) permeability constants of the tiles.

Condition	k_1 (m²)	k_2 (m)
Laboratory	1.29E-15 ± 3.87E-16	1.97E-12 ± 1.25E-12
Natural weathering	5.20E-16 ± 2.45E-16	4.90E-13 ± 1.59E-13

3.2. Changes in the mineral composition of the tiles

Fig. 8 depicts the main cementitious phases (detected by X-ray diffraction) present in the tiles aged in the internal environment of the laboratory. Other additional hydration products were identified in the tiles aged under external or natural weathering exposition (Fig. 9), which can be attributed to the continued hydration process when exposed to the weather. Calcium hydroxide ($Ca(OH)_2$) was not identified in both tiles, regarding that 5% by mass is the limit of the sensibility of the equipment. Such a result indicates that in both tiles (aged in laboratory or under natural weathering) it was occurred the adsorption of CO_2 in the cement based matrix and the consequent formation of calcite ($CaCO_3$) as stated in Tonoli et al. [19].

Diffuse peaks at 48.6°, 47.6° and 47.3° of both aged in laboratory and under natural weathering exposition, similarly to those reported by Cole and Kroone [23] confirmed the presence of poorly crystallized calcite. Anhydrous calcium silicate peaks were only found in the weathering exposed tile, as an indication that the matrix of this sample had not yet completely hydrated. The main peak of C–S–H (29.5°) is coincident with the main peak of calcite and calcium oxide in the specimen aged under natural weathering exposition. Peaks of high Ca/Si C–S–H [24] do not appear in the weathering exposed tile. Some cementitious phases (antigorite and gismondine) identified in the X-ray diffraction of the laboratory cured tile seem to be less stable in contact with the rainwater than calcite for example.

Thermogravimetric (TG) analyses from specimens under internal (laboratory) and external (natural weathering) exposition were applied to determine the mass losses, expressed as a percentage of the total fractions (Table 7). The main compounds that decompose thermally up to 350 °C are C–S–H, ettringite and gypsum [25,26], however this last two minerals were not identified in the X-ray diffractions. From about 350–450 °C, thermal decomposition of magnesium compounds takes place [16].

As presented in Table 7 the average amount of magnesium compounds in the tiles aged in laboratory was not significantly higher than that in the tiles under weathering exposition. Portlandite was not identified in the X-ray diffraction, however in the TG analyses the onset of an endotherm at about 450 °C is due to the $Ca(OH)_2$ formed from the further hydration of the C_3S phase [27] in the tile under natural weathering exposition (Fig. 9). Thermal decomposition of poorly crystallized calcite [23] occurs in the range between 500 and 800 °C [28] and of well-crystallized calcite at temperatures above 800 °C [24,29]. The C–S–H content (Table 7) of composites exposed to internal environment (laboratory) is less intense than the halos of the corresponding composites exposed to natural weathering. This relates to an increase in the amount

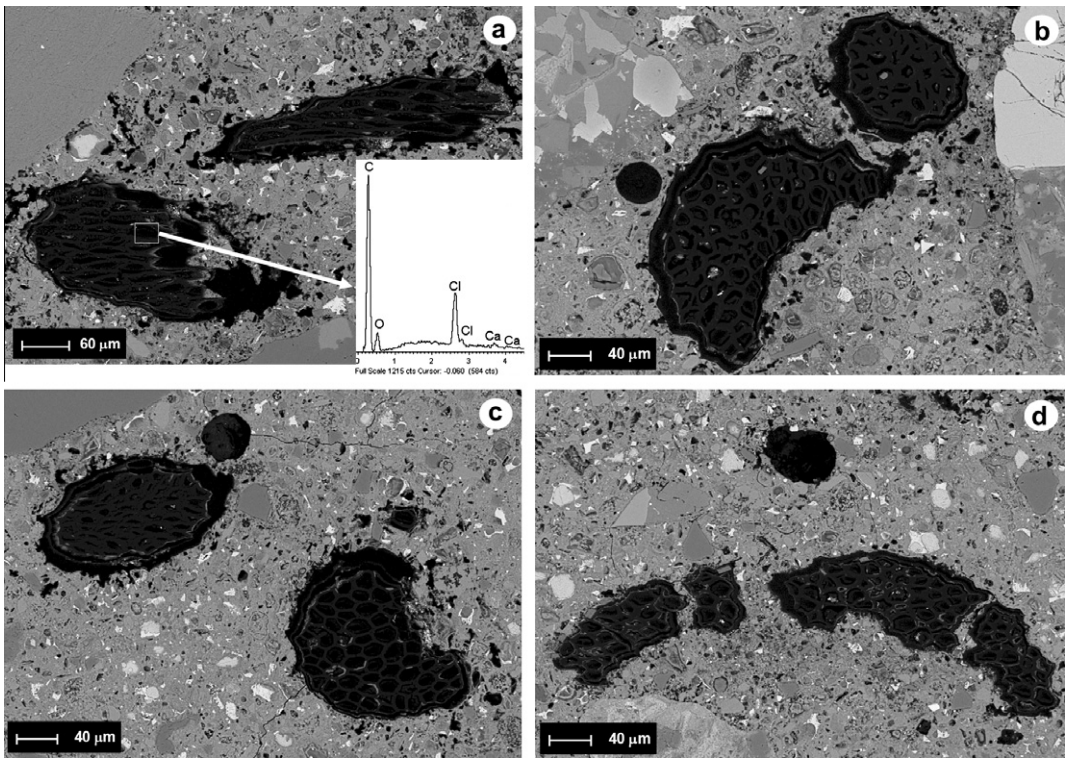

Fig. 6. SEM, back scattering electrons (BSE) image of the cross-sectioned fique fibre in 14 years old composite aged in protected environment (laboratory). EDS spectra was done in the fibre lumen.

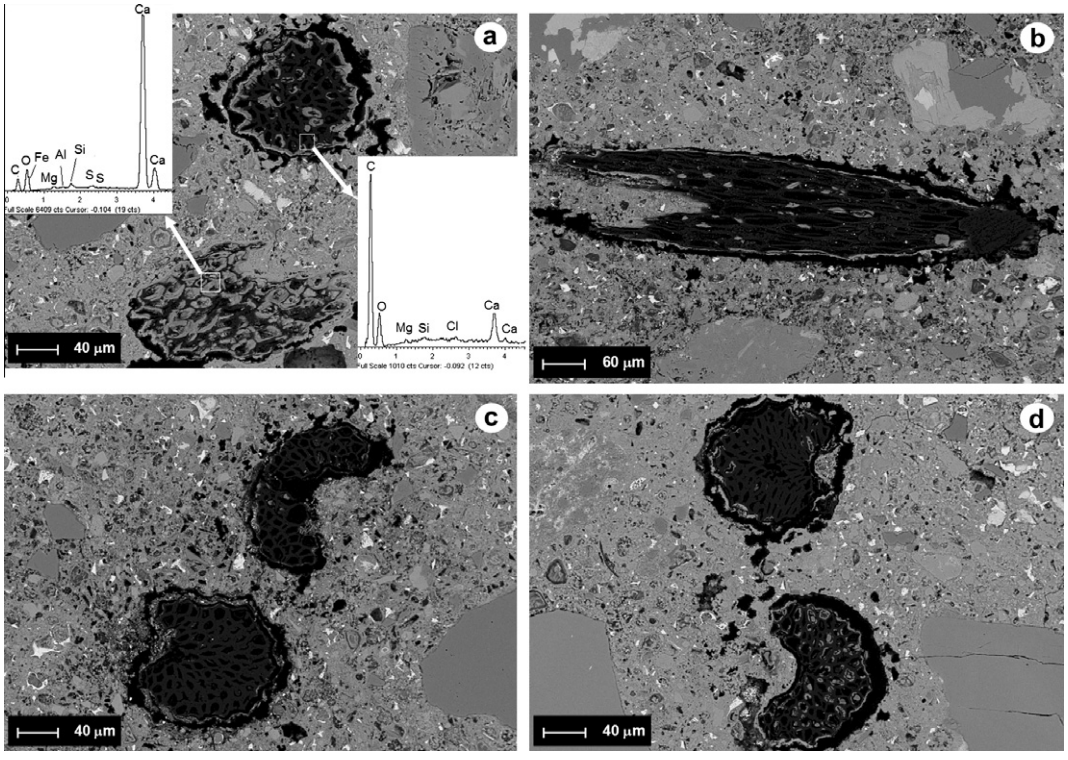

Fig. 7. SEM, back scattering electrons (BSE) image of the cross-sectioned fique fibre in 14 years old composite, aged under natural weathering exposition. EDS spectra was done in the fibre lumen.

of C–S–H when in contact with rainwater (natural weather exposition). Calcium sulphate dehydrate was not detected in the samples. The presence of calcium sulphate dehydrate is associated to ettringite carbonation reaction [16].

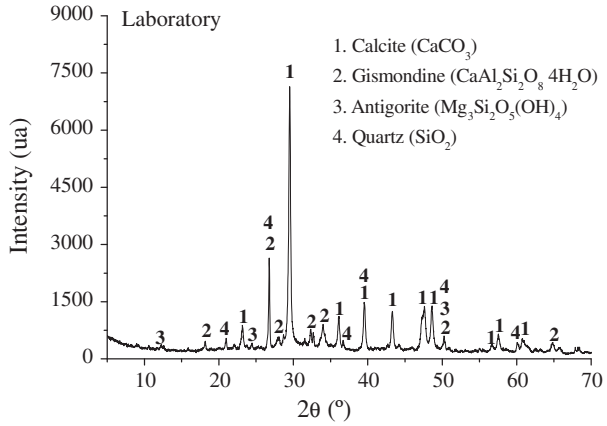

Fig. 8. X-ray diffraction pattern of the tile aged in the internal environment (laboratory).

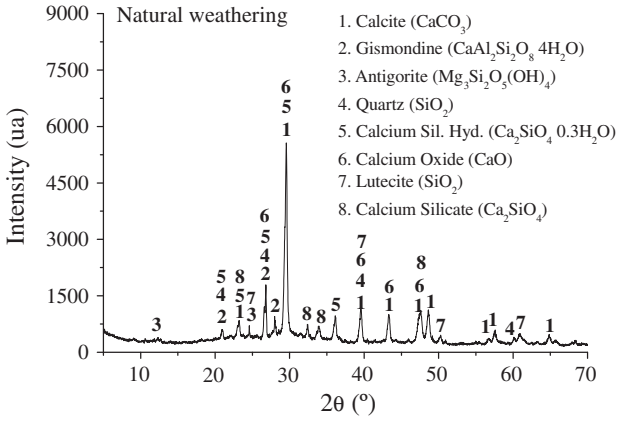

Fig. 9. X-ray diffraction pattern of the tile aged under external exposition.

Table 7
Loss of mass (%) on TG analyses.

Components	Laboratory	Natural weathering
C–S–H and sulfoaluminates	5.06 ± 1.36	5.82 ± 0.12
Magnesium compounds	1.68 ± 0.62	1.31 ± 0.30
Portlandite	0.74 ± 0.14	0.79 ± 0.16
Poorly crystallized carbonates	19.16 ± 1.88	20.44 ± 1.05
Well-crystallized calcite	0.56 ± 0.21	0.53 ± 0.07

4. Conclusions

The increase of the water absorption and apparent void volume in the fibre-cement roofing tiles aged under weathering exposition could be the consequence of the leaching of some less stable cementitious products, which decreased the bulk density of the specimens. Contrarily, the microstructure of the tiles aged under natural weathering presented lower air permeability than tiles aged in laboratory, due mainly to the increase in the tortuosity of the pore structure. Weathering exposed tiles exhibited a damaged fibre–matrix interface, as a consequence of the stresses caused by the fibre volume changes. This matrix microcracking close to the fibres led to the coarsening of pores greater than 100 nm differently from the pore distribution in the tiles aged in laboratory. Coarsening has been also associated with SiO_2 (gel) formation during carbonation of C–S–H and leaching of the cement matrix. As expected, other mineral phases were detected due to the continued hydration process of the matrix when tiles are exposed to the weather, which led to the increase of real density of the matrix and reduction of the pores lower than 100 nm. The present results contribute to the understanding of fibre-cement degradation, showing that the water uptake and release under 14 years of natural weathering led to damages in the fibre–matrix interface that may result in loss of strength of the tiles, and to the fibre mineralization that might cause embrittlement of the fibre-cement tiles after tropical weathering exposition.

Acknowledgments

The authors were supported by Grants offered by CNPq, Capes and Fapesp, Brazil, and by Colciencias and the Ministery of Agriculture and Rural Development, Colombia.

References

[1] Soroushian P, Marikunte S. High performance cellulose fiber reinforced cement composites. In: Proceedings of the international workshop high performance fiber reinforced cement composites. RILEM, E&FN SPON; 1992.
[2] Portland Cement Association. Fiber reinforced concrete, PCA; 1991.
[3] Coutts RSP. A review of Australian research into natural fibre cement composites. Cem Concr Compos 2005;27(5):518–26.
[4] Swamy RN. Influence of slow crack growth on the fracture resistance of fibre cement composites. Int J Cem Compos 1980;2(1):43–53.
[5] Gutierrez R, Delvasto S. Cabuya in cement composites, ceramic matrix composites and other systems. In: Proceedings of the ninth international conference on composite materials (ICCM/9). University of Zaragoza; 1993. p. 834–41.
[6] Alban F. Cabuya fiber mortar for corrugated tiles and flat sheets, ceramic matrix composites and other systems. In: Proceedings of the ninth international conference on composite materials (ICCM/9). University of Zaragoza; 1993. p. 830–3.
[7] Delvasto S, Toro EF, Perdomo F, Mejía de Gutiérrez R. An appropriate vacuum technology for manufacture of corrugated fique fiber reinforced cementitious sheets. Construct Build Mater 2010;24(2):187–92.
[8] Savastano Jr H, Agopyan V, Nolasco AM, Pimentel L. Plant fibre reinforced cement components for roofing. Construct Build Mater 1999;13(8):433–8.
[9] Delvasto S, Gutiérrez RM, Escándon AM. Mechanical properties of polymer portland cement concretes reinforced with steel, polypropylene, and fique fibers. In: Proceedings of the IAC-NOCMAT, João Pessoa; 2003.
[10] Savastano Jr H, Warden PG, Coutts RSP. Microstructure and mechanical properties of waste fibre–cement composites. Cem Concr Compos 2005;27:583–92.
[11] Kuder KG, Shah SP. Effects of pressure on resistance to freezing and thawing of fiber-reinforced cement board. ACI Mater J 2003:463–8.
[12] Mehta PK, Monteiro PJM. Concrete: microstructure, properties, and materials. 3rd ed. New York: McGraw Hill; 2006.
[13] Innocentini MDM, Pardo ARF, Pandolfelli VC. Modified pressure–decay technique for evaluating highly dense refractories permeability. J Am Ceram Soc 2000;83(1):220–2.
[14] Innocentini MDM, Pardo ARF, Menegazzo BA, Bittencourt LRM, Rettore RP, Pandolfelli VC. Permeability of high-alumina refractory castables based on various hydraulic binders. J Am Ceram Soc 2002;85(6):1517–21.
[15] Salomão R, Cardoso FA, Innocentini MDM, Bittencourt LRM, Pandolfelli VC. Polymeric fibers and the permeability of refractory castables. Cerâmica 2003;49:23–8 [In Portuguese].
[16] Dias CMR, Cincotto MA, Savastano Jr H, John VM. Long-term aging of fiber-cement corrugated sheets–The effect of carbonation, leaching and acid rain. Cem Concr Compos 2008;30(4):255–65.
[17] Bier TA, Kropp J, Hilsdorf HK. Carbonation and realkalinization of concrete and hydrated cement paste. In: Durability of construction materials 3, Proceedings of the 1st Congress from materials science to construction materials engineering, RILEM; 1987.
[18] Haga K, Sutou S, Hironaga M, Tanaka S, Nagasaki S. Effects of porosity on leaching of Ca from hardened ordinary Portland cement paste. Cem Concr Res 2005;35(9):1764–75.
[19] Tonoli GHD, Santos SF, Joaquim AP, Savastano Jr H. Effect of accelerated carbonation on cementitious roofing tiles reinforced with lignocellulosic fibre. Construct Build Mater 2010;24(2):193–201.
[20] Gram HE. Durability of natural fibres in concrete. In: Swamy RN, editor. Natural fibre reinforced cement and concrete (concrete technology and design 5). Glasgow: Blackie; 1988. p. 142–72.
[21] Coutts RSP. Wood fibre reinforced cement composites. In: Swamy RN, editor. Natural fibre reinforced cement and concrete (concrete technology and design, 5). Glasgow: Blackie; 1988. p. 208–42.
[22] Ramakrishna G, Sundararajan T. Studies on the durability of natural fibres and the effect of corroded fibres on the strength of mortar. Cem Concr Compos 2005;27:575–82.

[23] Cole WF, Kroone B. Carbon dioxide in hydrated Portland cement. J Am Concr Inst 1960;31:1275–95.
[24] Chen JJ, Thomas JJ, Taylor HFW, Jennings HM. Solubility and structure of calcium silicate hydrate. Cem Concr Res 2004;34(9):1499–519.
[25] Taylor HFW. Cement chemistry. Thomas Telford; 1997.
[26] Ramachandran VS. Applications of differential thermal analysis in cement chemical. New York: Chemical Publishing Company; 1969.
[27] Ramachandran VS, Beaudoin JJ. Handbook of analytical techniques in concrete science and technology. William Andrew Publishing, LLC Norwich: New Jersey: Noyes Publications, Park Ridge/New York; 1999.
[28] Gualtieri AF, Tartaglia A. Thermal decomposition of asbestos and recycling in traditional ceramics. J Eur Ceram Soc 2000;20(9):1409–18.
[29] Sato NMN. Porosity and mass transport on concrete. PhD thesis. Polytechnic School of University of São Paulo, São Paulo; 1998 [In Portuguese].